Low-power Physical-layer Design for LTE Based Very NarrowBand IoT (VNB - IoT) Communication

by

Prashant Sharma

A Thesis Presented in Partial Fulfillment
of the Requirements for the Degree
Master of Science

Approved November 2017 by the
Graduate Supervisory Committee:

Daniel W. Bliss, Chair
Chaitali Chakrabarti
Thomas McGiffen

ARIZONA STATE UNIVERSITY

December 2017

ABSTRACT

With the new age Internet of Things (IoT) revolution, there is a need to connect a wide range of devices with varying throughput and performance requirements. In this thesis, a wireless system is proposed which is targeted towards very low power, delay insensitive IoT applications with low throughput requirements. The low cost receivers for such devices will have very low complexity, consume very less power and hence will run for several years.

Long Term Evolution (LTE) is a standard developed and administered by 3^{rd} Generation Partnership Project (3GPP) for high speed wireless communications for mobile devices. As a part of Release 13, another standard called narrowband IoT (NB-IoT) was introduced by 3GPP to serve the needs of IoT applications with low throughput requirements. Working along similar lines, this thesis proposes yet another LTE based solution called very narrowband IoT (VNB-IoT), which further reduces the complexity and power consumption of the user equipment (UE) while maintaining the base station (BS) architecture as defined in NB-IoT.

In the downlink operation, the transmitter of the proposed system uses the NB-IoT resource block with each subcarrier modulated with data symbols intended for a different user. On the receiver side, each UE locks to a particular subcarrier frequency instead of the entire resource block and operates as a single carrier receiver. On the uplink, the system uses a single-tone transmission as specified in the NB-IoT standard.

Performance of the proposed system is analyzed in an additive white Gaussian noise (AWGN) channel followed by an analysis of the inter carrier interference (ICI). Relationship between the overall filter bandwidth and ICI is established towards the end.

To my family and friends

ACKNOWLEDGMENTS

I would like to thank my thesis adviser, Dr. Daniel Bliss for his constant support throughout my graduate studies. The door to Prof. Bliss's office was always open whenever I ran into a trouble or had questions about my thesis work. He consistently allowed this thesis to be my own work, but steered me in the right direction whenever he thought I needed it. I am also thankful to Dr. Chaitali Chakrabarti and Dr. Thomas McGiffen for serving on my committee and providing valuable comments on my thesis.

I am thankful to Dr. Daniel Bliss, Dr. Anna Scaglione, Dr. Chao Wang, Dr. Doug Cochran and Dr. Cihan Tepedelenlioglu of Electrical Engineering for teaching some of the important courses which built a strong foundation for conducting my research.

I am thankful to all my colleagues and co-workers at BLISS lab for their constant help and support in giving a good shape to this thesis. I learned a lot from those long technical discussions in the lab on a number of topics.

I am thankful to Karteek Rupakula, Ujjwala Kaushik, Alex Chiriyath, Aniket Katyayan for providing valuable feedback on my thesis.

I am grateful to my parents, Pawan Sharma and Geeta Sharma for always supporting me in every endeavor and my brother, Prateek Sharma for being my constant source of inspiration.

Finally, a big thank you to Siri Gowtham, without her support this thesis would not even be close to reality and my old friend, Sachin Grover for providing all the support during my graduate studies at Arizona State Univerity.

TABLE OF CONTENTS

CHAPTER Page

LIST OF FIGURES

LIST OF TABLES

Table Page

Chapter 1

INTRODUCTION

This chapter provides an introduction to the thesis by first developing the motivation behind the need to develop communication protocols for applications specific to Internet of Things (IoT). The purpose of thesis is defined next, followed by a problem formulation for a LTE based very low power wireless system for low throughput IoT applications. The problem is studied with specific scenarios under consideration and relies on a lot of underlying assumptions and hence the limitations of the study are discussed next. Finally, an outline for the rest of the thesis is provided.

1.1 Motivation

Over the past decade, there has been a tremendous growth in the number of wireless devices. As wireless technology matures, this number is expected to grow at an even higher rate with the goal being able to connect every physical device to the internet. This presents a huge opportunity for wireless system designers as 99.4 percent of the physical devices are still unconnected [2]. The idea behind IoT is to have a network of computing devices, vehicles, embedded systems with sensors etc which generate, exchange and process data intelligently and continuously. About 50 billion devices are estimated to be connected with IoT by 2020, up from about 200 million in the year 2000 and 10 billion in 2013 [2]. With such a massive number of devices connected to each other, machine to machine (M2M) communication is needed where devices would communicate with each other without any human interaction. It is expected that the revenue from M2M devices will grow from $200 million in 2011 to $1.2 trillion in 2022 [3]. Some of the services which might need machine

type communication (MTC) include consumer electronics, security and public safety, automotive, utilities, remote maintenance, payments, health and smart cities.

Until now, most of the wireless technologies were focused on improving the quality and performance of consumer electronic devices intended for human communication. MTC, however, is different from human communication as the throughput/delay/power requirement vary to a great extent based on the application and thus, require different connectivity solutions. While services involving consumer electronics, building security and maintenance can be served by a local area network (LAN), services such as remote maintenance (sensors, vending machines etc), utilities (power, gas, water, heating etc), smart cities etc need a wide area network (WAN) [4].

Since the cellular technology is pretty mature and is already deployed in most parts of the world, cellular based MTC systems can provide a solution for the IoT applications which need a WAN. LTE is one of the latest and widely accepted, high speed wireless communication standard by 3rd generation partnership project (3GPP) [5, 6]. The standard is revised regularly, in order to accommodate additional channel conditions and provide better connectivity with higher data rates and efficient resource utilization. However, LTE was designed for high speed communication and is not optimized for applications that need to support a potentially large number of low-rate, low power and delay tolerant devices. These low cost devices, typically used in applications such as sensors, remote maintenance and tracking, health-care, utilities etc, are expected to have very low complexity, low mobility and low power consumption with a very long battery life [4]. Hence, it is desirable to develop LTE based wireless systems, suitable for low data-rate and low power IoT applications.

1.2 Background

Realizing the importance of IoT for low-power and low cost applications with extended coverage and very long battery life, 3GPP introduced narrowband IoT (NB-IoT), as a part of their LTE-Release-13 [7–9]. Although NB-IoT is based on LTE, but it's a new radio-access technology as it is not fully backward compatible with the existing LTE devices. However, it can be easily integrated in the existing LTE network by allocating some of the time and frequency resources to NB-IoT.

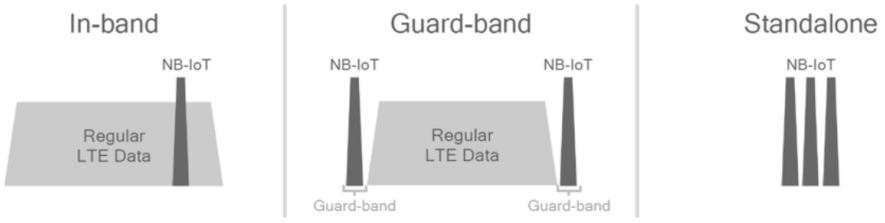

Figure 1.1: NB-IoT deployment modes [1]

With a bandwidth requirement of 180 kHz, three major deployment modes have been identified [10] for NB-IoT:

1. *Stand alone*, utilizing a 200 kHz band used by global gystem for mobile communication (GSM) frequencies

2. *Guard band*, occupying a 180 kHz wide physical resource block in the guard band of existing LTE carrier band

3. *In band*, occupying one physical resource block within the LTE carrier bandwidth.

Thus, NB-IoT reuses the existing LTE design with respect to physical layer processing which reduces the time required to develop the NB-IoT devices to a great extent.

1.3 Purpose

As discussed in the previous section, NB-IoT provides a provision to allocate a single resource block (RB) to each user, instead of at-least six resource blocks in existing LTE. A single RB corresponds to a bandwidth of 180kHz (and hence the name narrow-band) as compared to the minimum bandwidth of 1.4 MHz in conventional LTE systems. The resource block concept is discussed in later chapters.

The purpose of this thesis is to develop a new, low power, wireless communication system targeted towards IoT applications, having very low throughput requirements with relaxed transmission delay requirements. The overall system, similar to NB-IoT, will be based on LTE and will have very low complexity, consume very less power and have a long battery life. This system is able to allocate a very narrow bandwidth of 15 kHz to each user while retaining the existing LTE physical layer structure . We shall refer to this system as very narrowband IoT (VNB-IoT) system.

1.4 Problem Formulation

NB-IoT standard allocates one resource block per user irrespective of the throughput requirements of the application. A single resource block comprises of twelve subcarriers, each separated by 15kHz in frequency, giving a bandwidth of 180kHz. This might not be an efficient way of using the available spectrum when the throughput requirement is extremely low. In extreme cases, when the data-rate requirement is very low, we might as well allocate each subcarrier to a different user. This would enable a very efficient use of the available spectrum with a multiplexing gain of twelve.

The transmitter in this case will be a NB-IoT transmitter with each subcarrier carrying data for a separate user. A NB-IoT receiver, however, would not be a good solution as there is no need to process the entire 180MHz band when information per

user is contained only in the 15kHz band. Also, since a Fast Fourier Transform (FFT) block consumes a good amount of power, throwing away an FFT block from the receiver would save a lot of power and result in a much longer battery life.

Keeping the above things in mind, we propose a simple single carrier based receiver architecture, where each receiver is locked only to a particular subcarrier frequency and not to the entire 180 kHz band. This can be achieved by putting a narrowband filter around the desired subcarrier. However, since the subcarriers are tightly packed in frequency, a very narrowband filter with a sharp transition band is needed to avoid any interference from the adjacent subcarriers which is expensive and draws a lot of power. We propose a multi-stage filtering approach with each stage separated by a down-sampling process. The proposed approach, however, introduces inter-(sub)carrier-interference (ICI) and hence degrades the receiver performance.

Next, we design the complete receiver and study it's performance in an additive white Gaussian noise (AWGN) channel. We shall study the extent of degradation for a particular set of filters along with the nature of the interference noise. In the end, we study how the interference changes with filter bandwidth.

1.5 Limitations

In this thesis, we study the physical layer properties of the receiver architecture, with a focus on the downlink path of the system. Problems related to resource allocation and higher layer management are not discussed as a part of the thesis. Further, since the target data-rate and power requirements are low, a single antenna based solution is considered. Only lower order modulation schemes, for instance, binary phase-shift keying (BPSK) and quadrature phase-shift keying (QPSK), provide a satisfactory performance because of the non-negligible ICI, resulting from a performance-complexity trade-off.

1.6 Outline

The remainder of this work is outlined as follows.

Chapter 2 provides a brief overview of OFDM, which is the underlying technology behind LTE based systems. Apart from basic principles, various factors that contribute to the design of an OFDM waveform are discussed. Next, typical OFDM transmitter and receiver processing blocks are discussed, including some of the channel estimation and equalization techniques that are employed. Finally, a discussion on two of the main challenges encountered in OFDM is provided.

In Chapter 3, a discussion on various transmitter blocks used in the LTE physical layer is provided. These include modulation and coding schemes, scrambling, resource block allocation and physical layer signals. By making slight changes to these blocks, the proposed transmitter model for VNB-IoT is discussed. The model is derived from NB-IoT, which is the latest LTE standard for IoT. Wherever possible, the major differences between the three standards are highlighted .

In Chapter 4, a simple receiver design is provided for the VNB-IoT system proposed in the thesis. All the major blocks in the receiver processing, including the RF front end, synchronization, channel estimation and equalization, descrambling, demapping and viterbi decoding, are discussed.

Chapter 5 provides a MATLAB based simulation model for VNB-IoT transmitter and receiver. Performance in AWGN channel is dicussed along with an estimation process for the interference noise. The dependence of ICI on filter bandwidth is described towards the end of the chapter.

Finally, Chapter 6 gives a summary of the work done as a part of the thesis, followed by a discussion on some of the future work that can be done in this direction.

Chapter 2

ORTHOGONAL FREQUENCY DIVISION MULTIPLEXING

Most of the wireless communication systems are multi-user systems. Given the limited radio resources, the available frequency spectrum needs to be shared among multiple users. There are various multiple access schemes such as

1. Time division multiple access (TDMA)
2. Code division multiple access (CDMA)
3. Frequency division multiple access (FDMA)
4. Space division multiple access (SDMA)
5. Carrier sense multiple access (CSMA)

Orthogonal frequency division multiple access (OFDMA) is a special kind of FDMA scheme in which the carriers are structured in such a way that they don't interfere with each other, i.e. they are orthogonal to each other. The underlying technology behind OFDMA is that of OFDM. This chapter discusses the basic principles of OFDM and various factors that contribute to the design of an OFDM waveform.

2.1 Basic principles of OFDM

OFDM works on the principle of dividing a wideband signal into multiple narrowband 'orthogonal' signals all transmitted at the same time and using the same antennas. This is similar to a frequency division multiplexing (FDM) except for the fact that the carriers are spaced much closer in frequency with no guard band in

between, thus increasing the spectral efficiency. The placement of these multiple carriers, also known as subcarriers, is done in a way that they do not interfere with each other during the sampling time instant and hence can be separated at the receiver despite their overlapping spectrum. (Figure 2.1) shows how the subcarriers are placed. The orthogonality of the subcarriers is maintained by keeping the frequency separation($\Delta f = f_{k+1} - f_k$) as inverse of the OFDM symbol duration (T). i.e.

$$\Delta f = 1/T \tag{2.1}$$

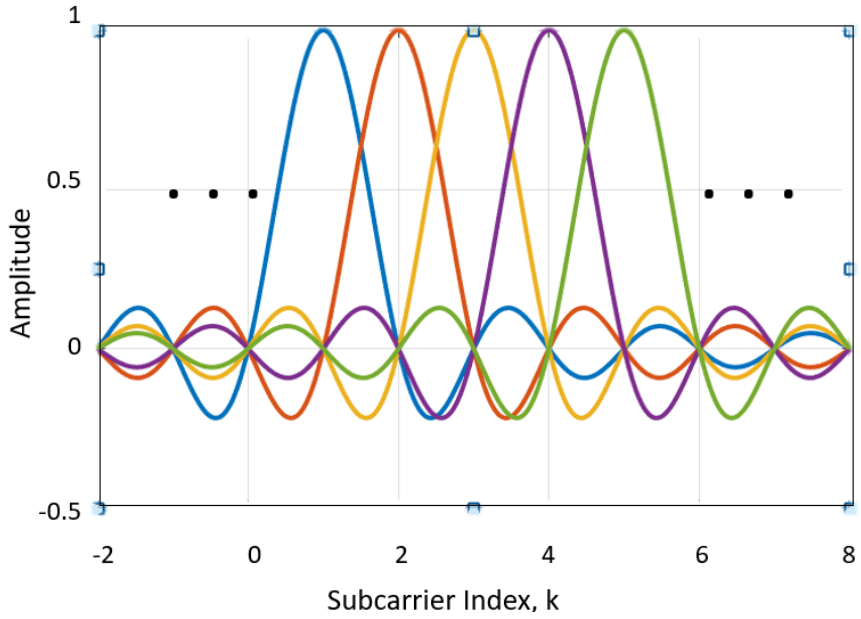

Figure 2.1: The orthogonality of the OFDM subcarriers is maintained by keeping a frequency separation, $\Delta f = f_{k+1} - f_k = 1/T$, where T is the OFDM symbol duration

An OFDM signal is generated by summing up multiple orthogonal sub-carriers which are modulated by the data symbols drawn from a particular constellation. The time domain OFDM symbol, $x[n]$, of length N can be written as

$$x[n] = \sum_{k=0}^{N-1} s_k \exp(j2\pi nk/N) \qquad n = [0, 1, ..., N-1] \tag{2.2}$$

where s_k denotes the modulation symbols, k denotes the subcarrier index and N is the total number of subcarriers. This operation can be performed efficiently by making use of an N-point inverse fast-fourier-transform (IFFT). Although an OFDM signal uses N subcarriers, not all of them are loaded with information. Subcarriers around $\pm\frac{f_s}{2}$ are usually set to zero to avoid adjacent channel interference (ACI). Also, the DC subcarrier is also set to zero in order to simplify the analog-to-digital converter (ADC) and digital-to-analog converter (DAC) operations.

The sampling time, T_s is given by

$$T_s = T/N = \frac{1}{N\Delta f} \quad , \tag{2.3}$$

and hence the sampling rate, $f_s = \frac{1}{T_s} = N\Delta f$.

2.2 Subcarrier Spacing

The number of subcarriers in a typical OFDM symbol can vary over a range between less than a few hundreds to a few thousands. The sub-carrier spacing ranges from a few kHz to hundreds of kHz. As mentioned in the previous section, sub-carrier spacing is related to the length of the OFDM symbol as seen in Equation (2.1), and hence is an important parameter in OFDM system design. Subcarrier spacing is decided by considering various aspects of the environment such as the maximum delay spread and maximum Doppler spread.

Delay spread of the channel determines the coherence bandwidth, i.e. the range of frequencies over which the channel de-correlates [11]. A channel can be assumed to be almost flat during the coherence bandwidth. This puts a limit on the maximum subcarrier spacing the system can have without a major degradation of the signal.

Doppler spread determines the coherence time of the channel [11]. This is the time over which the channel can be assumed to be highly correlated. It's desirable to

keep the OFDM symbol duration within the coherence time. This puts a lower limit on the subcarrier spacing.

It is desired to have the subcarrier spacing as small as possible to minimize the cyclic prefix overhead. A very small subcarrier spacing, however, increases the sensitivity of the OFDM symbol transmission to any kind of frequency synchronization issues resulting from Doppler spread or oscillator frequency mismatch. Once the subcarrier spacing has been selected, the number of subcarriers can be determined based on the available channel bandwidth. However, as mentioned previously, not all of these subcarriers may be used to carry information symbols. Few subcarriers near the edge of the spectrum and around DC are kept unused.

2.3 Cyclic Prefix

Due to multipath propagation, the wireless channel is, almost always, time-dispersive in nature. This leads to delayed replicas of past OFDM symbols interfering with the current symbol, a phenomenon called inter symbol interference (ISI). In order to combat ISI and make the OFDM symbols insensitive to time-dispersion, a guard interval is provided in between the OFDM symbols. The length of the guard interval is selected to be more than the maximum delay spread of the channel. As a possible solution, the last few samples of the OFDM symbol are copied and added to the beginning of the symbol to serve as guard interval [11]. This type of guard insertion is known as cyclic prefixing, which is shown in Figure 2.2. Using the cyclic prefix as a guard interval has few other advantages in terms of changing the linear convolution with the channel to circular convolution which enables a single tap frequency domain equalization as discussed in next section.

Since the samples corresponding to the cyclic prefix gets corrupted because of ISI, they are usually dropped at the receiver. There is no loss of information in doing so

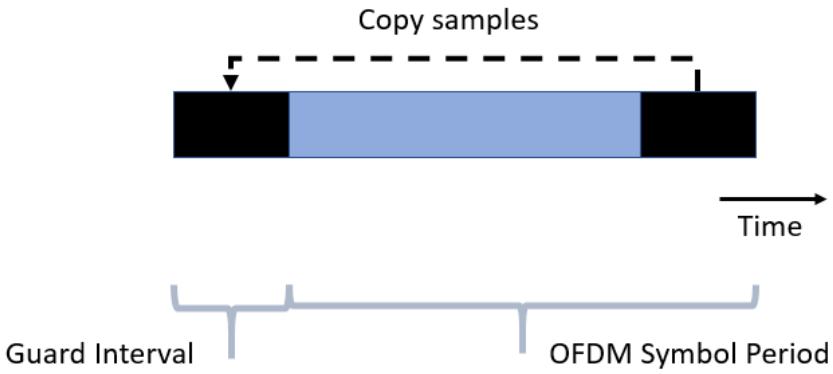

Figure 2.2: The last few samples of the OFDM symbol are copied and added to the beginning of the symbol to serve as guard interval. This type of guard interval is called as cyclic prefix.

as the cyclic prefix carries redundant information. Adding a cyclic prefix, however, comes at a cost in terms of increased signal overhead and, as a result, reduction in data-rate. Furthermore, the transmit power used for sending cyclic prefix samples is wasted as the samples are dropped at the receiver. Hence, there is a trade-off in selecting the duration of cyclic prefix.

2.4 OFDM transmission system

Figure 2.3 shows a typical OFDM transceiver system. The payload bits are modulated by a PSK/QAM modulator based on some modulation scheme, for instance, BPSK, QPSK, QAM16, QAM 64 etc, resulting in a sequence of complex symbols. A serial-to-parallel convertor, then, takes N of these symbols and gives out a set of N parallel symbols, to be transmitted on a set of N subcarriers. An IFFT block converts these frequency domain signals into the time domain, as mentioned in Equation (2.2), followed by the addition of a cyclic prefix after serializing the IFFT output through a parallel-to-serial converter.

The generated baseband sequence is then converted to an analog signal, filtered,

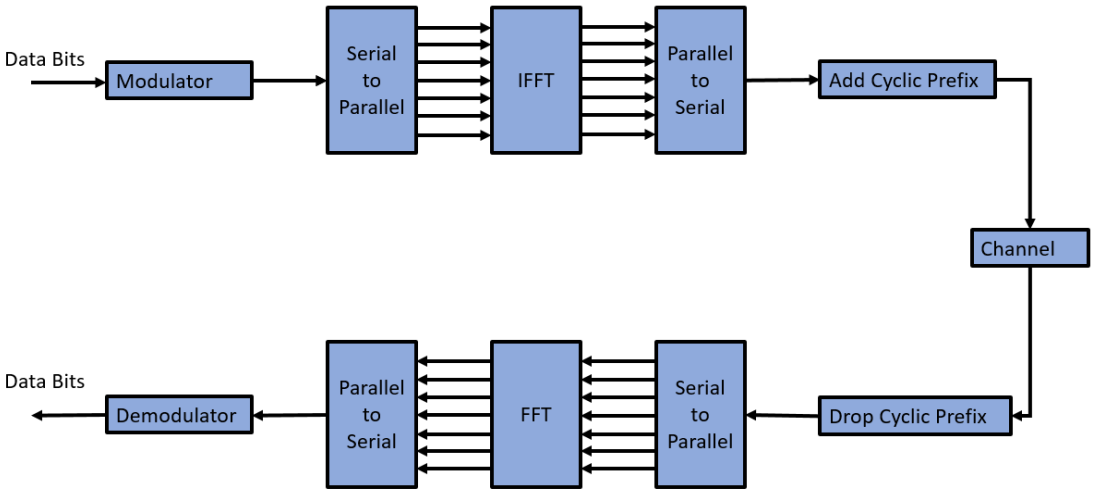

Figure 2.3: OFDM with IFFT/FFT implementation

up-converted, amplified and transmitted via single or multiple antennae. The transmitted signal after passing through a wireless channel is received by single/multiple antenna as a filtered signal, corrupted with additive noise. The signal is then down-converted to baseband and filtered to remove any higher frequency components. An ADC then converts the analog signal to discrete samples to be processed by a digital receiver. All this processing can be represented by a discrete channel, $h[n]$ which takes a discrete sequence, $x[n]$, as input and gives out a discrete sequence, $y[n]$, as output along with AWGN, $\nu[n]$, as shown by

$$y[n] = x[n] * h[n] + \nu[n] \qquad -\mu \leq n \leq N-1 \quad , \tag{2.4}$$

where μ is the number of samples per symbol used for the cylic prefix.

The cyclic prefix is then removed to obtain N samples in time, for each OFDM symbol. A serial to parallel converter parallelizes the stream of cyclic-prefix removed samples into blocks of FFT length, N. These blocks of samples are then converted to frequency domain by emplyoing a FFT. The resulting frequency domain symbols are then passed to a demodulator which extracts the payload bits out of the symbols.

2.5 Channel Estimation and Equalization

As discussed in the previous section, the transmitted signal undergoes a wireless channel before being captured by a receive antenna. Wireless channel has adverse effects of introducing distortions to the signal, a phenomenon known as fading [11, 12]. The amount of fading varies across the bandwidth of the signal and hence, all the frequencies gets attenuated by different levels of magnitude and phase. However, in OFDM, entire bandwidth is divided into multiple narrow bands such that the channel response is almost flat within each narrow band [11–14]. This can be represented as

$$Y[k] = H[k]X[k] + V[k] \qquad 0 \leq k \leq N-1 \quad , \tag{2.5}$$

where $Y[k]$ represents the received constellation symbol on k^{th} subcarrier when $X[k]$ was the transmitted. $H[k]$ and $V[k]$ represents the flat fading complex gain and AWGN, respectively, for k^{th} subcarrier. If the channel gains $H[k]$ are known for each subcarrier, the original transmitted symbol can be estimated as:

$$\hat{X}[k] = Y[k]/H[k] + V[k]/H[k] \qquad 0 \leq k \leq N-1 \tag{2.6}$$

This process, known as frequency equalization, removes the effects of flat fading channel on each subcarrier, independently. Frequency domain equalization reduces the complexity of the receiver by a huge amount as it requires only a single multiplier per subcarrier (1-tap equalization) as compared to a long filter which is needed for time domain equalization.

The channel estimation process is typically carried out by sending a reference signal also referred to as pilot signal at regular intervals within the OFDM signal. These reference signals, which are known to the receiver are then used to estimate the channel.

2.6 Challenges in OFDM

With the advantages of high spectral efficiency, tolerance to frequency selective fading, simple equalization process, etc, OFDM do offer few challenges to tackle. The two main challenges are - high peak-to-average power ratio (PAPR) and sensitivity to frequency and timing offsets.

2.6.1 Peak-to-Average Power Ratio

The PAPR of transitted signal in a wideband signal is defined as the ratio of maximum power of a sample to the average power of the signal [11], i.e.

$$PAPR_{dB} \triangleq 10log_{10}\frac{max_n|x[n]|^2}{\boldsymbol{E}_n[|x[n]|^2]}(dB) \quad , \tag{2.7}$$

where $\boldsymbol{E}[.]$ denotes the expectation operator. It is desired to have a low PAPR for an efficient use of the transmit power amplifier as a higher PAPR forces the power amplifier to have a large backoff in order to operate in the linear region. However, in OFDM based systems, PAPR grows linearly with the number of subcarriers, N, resulting from the coherent addition of all the subcarriers [11].

There are a number of efficient methods of reducing PAPR for OFDM signals. Some of these include clipping, peak cancellation, tone reservation, special coding techniques etc [15–19].

2.6.2 Frequency and Timing Offset

The efficiency of an OFDM system lies in maintaining the orthogonality of the subcarriers. As shown in Figure 2.1, the subcarriers are placed with a frequency separation as inverse of the OFDM symbol duration (Equation (2.3)). Any kind of offset in frequency and timing, causes deviation from this norm, resulting in a loss of orthogonality and severe degradation in performance because of ICI. In order to

tackle the ICI, both, the frequency and timing offsets are estimated and corrected at the receiver [20–24].

2.7 Summary

This chapter provided a brief overview of the OFDM systems which forms the backbone of any modern day wireless communication systems including LTE, WLAN, DSL etc. The underlying principle of OFDM was discussed, along with a typical transmitter and receiver processing blocks including channel estimation and equalization. Two main challenges in OFDM, high PAPR and sensitivity to timing and frequency offsets were discussed towards the end of the chapter.

Chapter 3

TRANSMITTER

As discussed in Chapter 1, the VNB-IoT system proposed in this thesis is based on LTE and NB-IoT standards. This chapter provides an overview of the LTE based, basic transmitter architecture used in the proposed VNB-IoT system. Since VNB-IoT does not use all the data/signal processing blocks specified in LTE standard, we shall restrict our discussion only to the blocks which are used in the proposed system. For a complete understanding of the LTE or NB-IoT standard, reader can refer to any standard book on LTE [5, 6, 25–27] or recent papers on NB-IoT [4, 7–10, 28]. The chapter begins with a discussion on basic transport and physical layer blocks of VNB-IoT, including modulation and coding, scrambling, resource grid and two important physical layer signals - synchronization signals (primary synchronization sequence (PSS) and secondary synchronization sequence (SSS)) and reference signals (CSR). The major differences/changes between LTE, NB-IoT and the proposed VNB-IoT system are presented along the context. The chapter ends with a description of a simple transmitter block diagram and a discussion on how the system works.

3.1 Modulation Schemes

The modulation schemes used in LTE include QPSK, 16-QAM (Quadrature Amplitude Modulation) and 64 QAM. NB-IoT uses QPSK as the only modulation scheme. For our VNB-IoT system, we shall use BPSK and QPSK and hence we'll limit our discussion about modulation schemes only to BPSK and QPSK.

BPSK is the most simple phase-shift-keying (PSK) modulation scheme. It takes a single bit at a time and maps it to one of the two constellation points which are

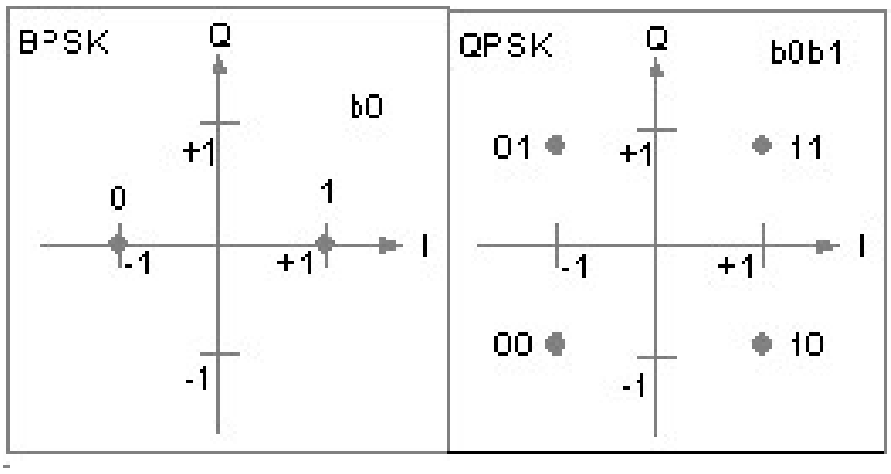

Figure 3.1: Two modulation schemes are proposed for VNB-IoT system, BPSK and QPSK. BPSK takes bit b_0 and maps it to ± 1 depending on whether it takes value 0 or 1. QPSK takes two bits $b_0 b_1$ and maps it to one of the four values $\pm 1 \pm j$ depending on the bit combination

180° apart. QPSK on the other hand takes two bits at a time and maps to one of the four constellation points spaced equally apart on a circle. Thus, QPSK achieves twice the data rate as compared to BPSK. Figure 3.1 shows the bit mapping for both of these modulation schemes. When the channel is good, i.e. signal-to-noise ratio (SNR) is relatively high, QPSK is used to achieve a higher throughput while in low SNR scenarios, BPSK is preferred because of its higher tolerance to noise.

3.2 Channel Coding

A wireless communication system uses channel coding to provide immunity against the channel errors at the cost of a reduced data rate. Redundant bits are added along with the data bits which helps in detection and/or correction of bit errors occurred during the transmission process. There are two main categories of channel codes - convolutional codes and block codes.

Convolutional codes takes into account the previous information bits along with the present information bits while generating the parity bits. Block encoder, on the

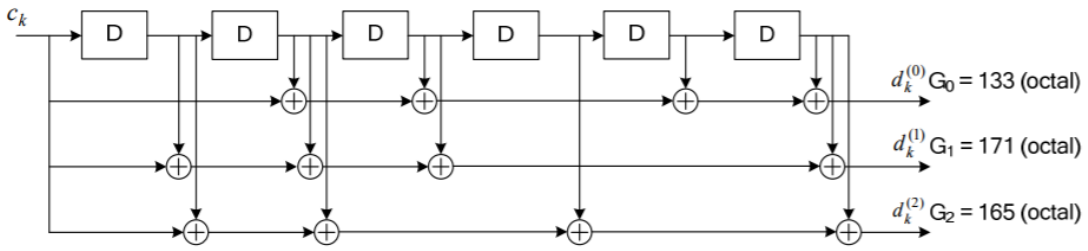

Figure 3.2: Rate 1/3 tail biting convolutional encoder

other hand, takes a block of information bits and appends parity bits to it. The parity bits are generated by using a generator matrix along with the input block of information bits.

LTE uses a different class of code, known as 'turbo code', which combine two convolutional codes separated by an interleaver. Since, the decoding process for a turbo code is highly complex, it may not be the best choice for IoT applications where complexity and power consumption are a big concern. For our VNB-IoT system we shall use a tail biting convolutional code with rate 1/3, which is also used by NB-IoT standard.

As shown in Figure 3.2, a rate 1/3 convolutional encoder takes a single information bit, c_k, and gives out three parity bits, $d_k^{(0)}$, $d_k^{(1)}$ and $d_k^{(2)}$, according to generator polynomials $G_0 = 133_8$, $G_1 = 171_8$ and $G_2 = 165_8$ respectively. The initial 6 values of the shift register are set to the values corresponding to the last 6 information bits in the input bit stream. This makes the initial and final states of the shift register to be the same.

3.3 Resource Mapping

In LTE, data is arranged on a time-frequency plane, also known as resource grid. The x-axis of the grid represents time (OFDM symbol index) while the y-axis repre-

sents frequency (subcarrier index). For a complete understanding of LTE and hence, NB-IoT and VNB-IoT, it is very important to understand the structure of the resource grid, various signals/channels that map to resource grid and how it is transformed into stream of time domain OFDM symbols. We discuss all these concepts in the following subsections.

3.3.1 Resrource Grid Design

The resource grid represents time on the x-axis and frequency on the y-axis.

In it's time domain structure, each LTE frame is 10ms long and comprises of 10 subframes, each of 1ms duration. The subframes are further divided into two time-slots of 0.5ms, each comprising 7 OFDM symbols in normal cyclic prefix operation and 6 OFDM symbols in extended cyclic prefix mode. For the sake of simplicity, we shall restrict our discussion only to normal cyclic prefix mode. A fixed subcarrier spacing of 15kHz gives an OFDM symbol duration of 66.67μs. A cyclic prefix of duration 5.2μs is used for the first OFDM symbol and 4.68μs for the rest of the symbols in each time-slot. This gives a total symbol duration of 71.87μs for the first symbol and 71.35μs for the rest of the symbols in a time-slot.

In frequency domain, each OFDM symbol is made up of a number of subcarriers depending upon the bandwidth allocated to the system. Irrespective of the bandwidth, the subcarrier spacing is maintained to be 15kHz for normal cyclic prefix operation. A single time-slot (i.e. 7 OFDM symbols) having 12 subcarriers forms a RB and is the basic building block of the resource grid for LTE. Thus, a single resource block has a bandwidth of 180kHz and a duration of 0.5ms. Depending on the available bandwidth, multiple RBs can be allocated for a single user for a given time-slot. Table 3.1 lists the number of RBs allocated for each of the possible bandwidths specified in LTE.

Table 3.1: Channel bandwidths and number of RBs specified in LTE

Channel Bandwidth (MHz)	Number of RBs
1.4	6
3	15
5	25
10	50
15	75
20	100

As seen in Table 3.1, LTE specifies a minimum bandwidth of 1.4 MHz per user. However, certain IoT applications do not demand a high throughput, but need to support a comparatively large number of user equipment (UE)s. Allocating such high bandwidth would not not only lead to spectral wastage, but also puts a limit on the number of users a base-station can support. This issue was addressed by 3GPP in LTE Release-13 with the introduction of NB-IoT which allows an allocation of a single RB to each user. Thus, NB-IoT symbol has a narrow bandwidth of 180kHz and hence allows a higher order of multiple-access. Our proposed system, VNB-IoT, takes this idea of resource allocation to the limiting case of allocating a single resource element (a single subcarrier within an OFDM symbol) to each user. Thus, VNB-IoT system allows a very narrow bandwidth of 15 kHz and can support about ten times more users simultaneously as compared to NB-IoT. Figure 3.3 describes the overall frame structure of the system along with the resource block allocation.

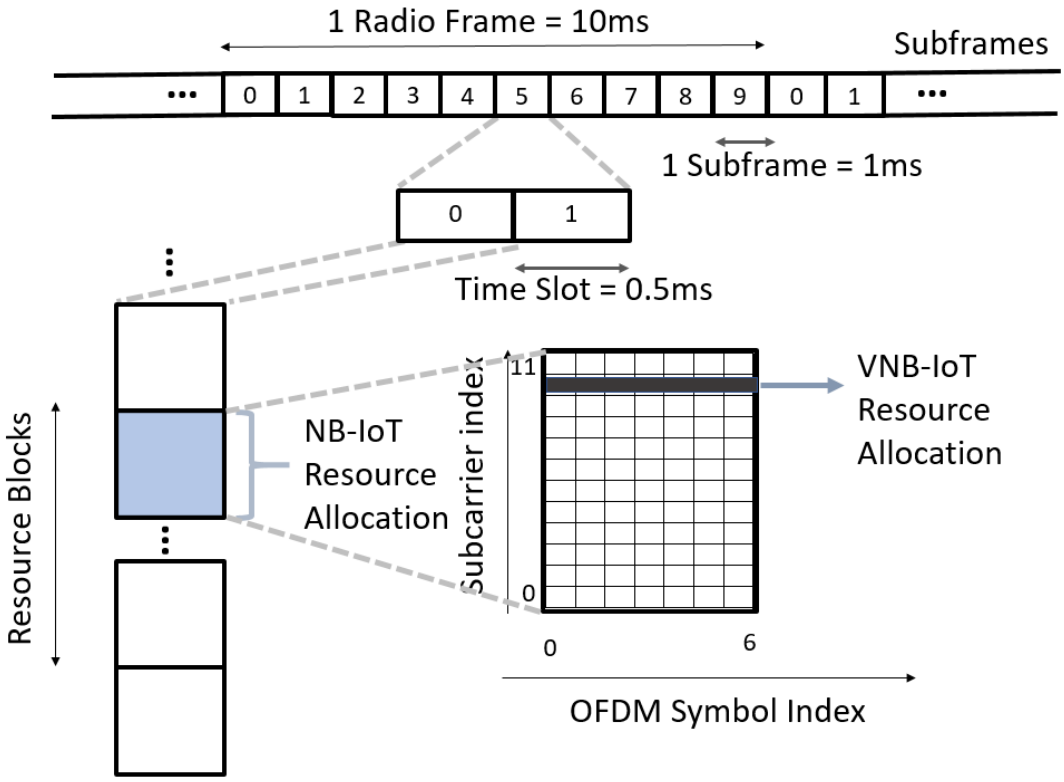

Figure 3.3: Resource block allocation in NB-IoT and VNB-IoT

3.3.2 Resource Grid Content

In the previous section, we discussed a basic structure of the resource grid on both time and frequency axes. Next, we discuss the types of data symbols that occupy the resource elements in the grid. In the downlink operation, there are mainly four different types of information contained in the resource grid - the modulation symbols corresponding to data bits, control information related symbols, reference symbols and synchronization symbols. In LTE, these signals can be attributed to either, one of the physical channels, i.e. Physical Downlink Shared Channel (PDSCH), Physical Downlink Control Channel (PDCCH) and Physical Broadcast Channel (PBCH), or physical signals, namely, cell-specific reference signal (CRS), PSS or SSS(Table 3.2). In the following sub-section, we discuss, in brief, the structure and placement of the

physical signals.

Table 3.2: NB-IoT physical channels and physical signals

Physical Channel	Purpose
PBCH	System information and frame number
PDCCH	Scheduling, ACKs etc
PDSCH	Payload data
Physical Signal	**Purpose**
Reference signals	Channel Estimation
PSS	Frame boundary detection
SSS	Frame number and cell ID

Reference Signals

In LTE, CRS are sent in every downlink subframe and in every resource block in the frequency domain. CRS are used by the UE to estimate the channel response for coherent demodulation of the physical channels. The generation of reference signals is not discussed in this thesis. Readers may refer to any standard book on LTE, [5, 6, 25–27, 29–32], to understand the process of reference signal generation. For a single antenna case, there are four CRS symbols per resource block - two in each of the 1^{st} and 5^{th} OFDM symbols. On frequency axis, the CRS symbols are separated by 6 subcarriers. Further, there is an offset of 3 subcarriers in the CRS corresponding to 1^{st} and 5^{th} OFDM symbols, Figure 3.4. A similar design can be employed for reference signal generation for VNB-IoT as well. Since, VNB-IoT occupies only one subcarrier, a reference symbol has to be sent in every time-slot.

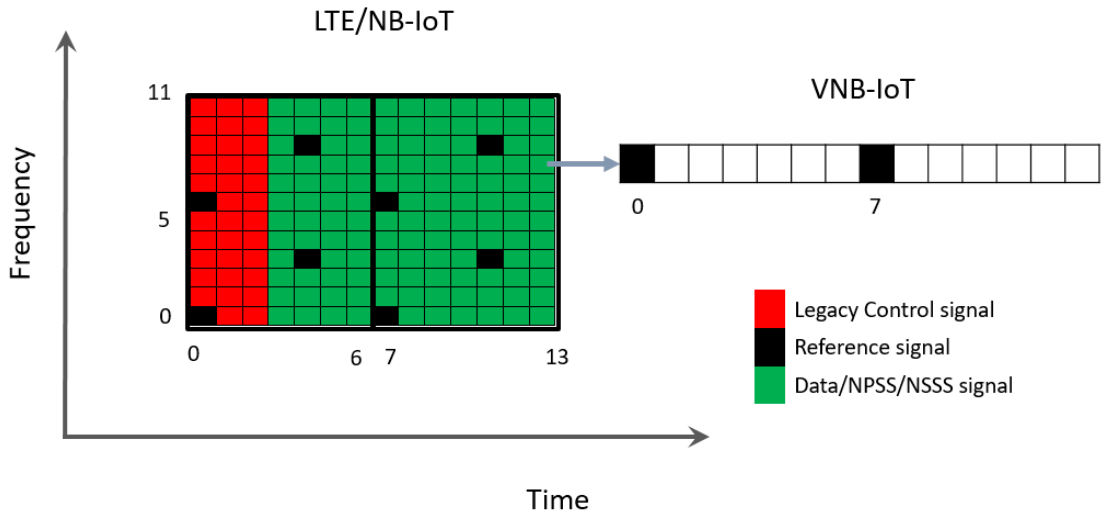

Figure 3.4: Reference signals in LTE/NB-IoT and VNB-IoT

Synchronization Signals

LTE defines synchronization signals to be used for various purpose such as cell search, frame boundary detection and time and frequency offset estimation. Two types of sychronization signals are defined - PSS and SSS. In LTE, the PSS and SSS are transmitted in the 7^{th} and 6^{th} OFDM symbols, respectively occupying the center 72 subcarriers in the resource grid during subframe 0 and 5. This means that the synchronization sequence is spread across 6 resource blocks. However, NB-IoT allocates a single resource block per user, hence, the design was updated to allocate an entire subframe for narrowband PSS (NPSS) or narrowband SSS (NSSS) transmission (Figure 3.4) to maintain a good quality of frame detection.

Both NPSS and NSSS are constructed as a concatenation of short Zadoff-Chu sequences. A length-11 base sequence along with a code cover comprising of a binary sequence of length 11 is used to generate the NPSS sequence while NSSS is generated by using the same base sequence with different root-indices and cyclic shift [33–35].

Taking a step further, VNB-IoT allocates a single subcarrier to each user and hence the synchronization sequence has to be extended to multiple sub-frames (a possible extension could be up-to 10 subframes (one frame)). This can be achieved by extending the length of code cover from 11 to 110 (=11x10). Optimizations can be done to obtain a code cover with good autocorrelation properties.

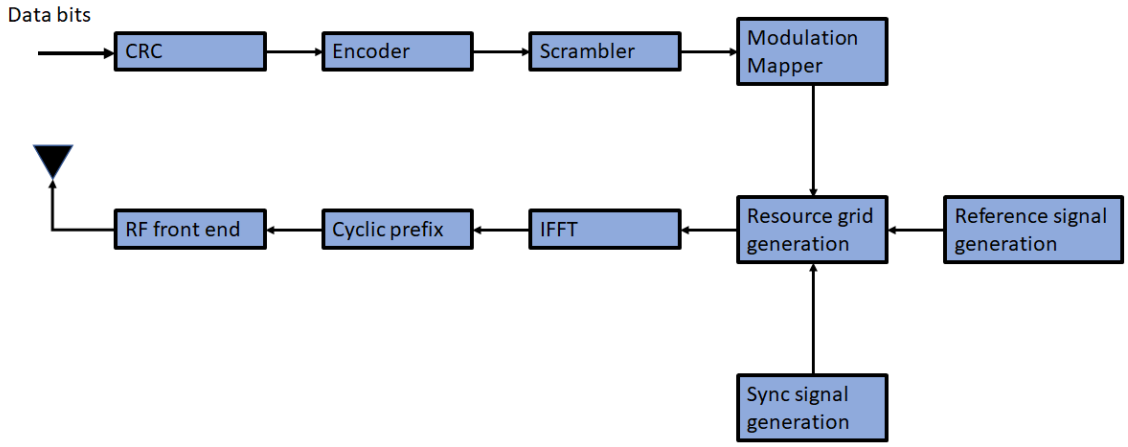

Figure 3.5: Basic transmitter block diagram

3.4 Transmitter

Figure 3.5 provides a block diagram of a simplified transmitter for the proposed VNB-IoT system. In the first step of the physical layer processing, a 24-bit cyclic-redundancy-check (CRC) is calculated and appended to the block of data provided by the multiple access channel (MAC). The data bits are then encoded with a rate-1/3 convolutional encoder as described in Figure 3.2 followed by scrambling with a bit-level scrambling sequence. The scrambled bits are then mapped to complex symbols based on one of the modulation schemes - BPSK or QPSK, as described in Section 3.1. Next, the resource grid is generated by allocating the data symbols, reference symbols and the synchronization symbols to their respective subcarriers. The resource grid is then transformed into time samples using an IFFT followed by

cyclic prefix insertion. The resulting stream of complex samples is then converted to the analog domain where it passes through filters, mixer and power amplifier and finally transmitted via an antenna.

3.5 Summary

In this chapter, we provided a brief description of various blocks in an LTE and NB-IoT transmitter. We described the frame format and resource grid structure and discussed how NB-IoT is derived from LTE and VNB-IoT from NB-IoT. Finally, a block diagram of a basic transmitter for VNB-IoT was provided with a description of the actual transmitting process.

Chapter 4

RECEIVER

In this chapter we provide a simple receiver design for the VNB-IoT system. The proposed receiver architecture is based on traditional single carrier receivers and is different from LTE and NB-IoT as it doesn't use a FFT for the demodulation process. This decreases the receiver complexity and power requirements as FFT consumes a lot of power and hardware. Figure 4.1 provides the block diagram, of a basic VNB-IoT receiver. The rest of the chapter provides a brief discussion on each of these blocks.

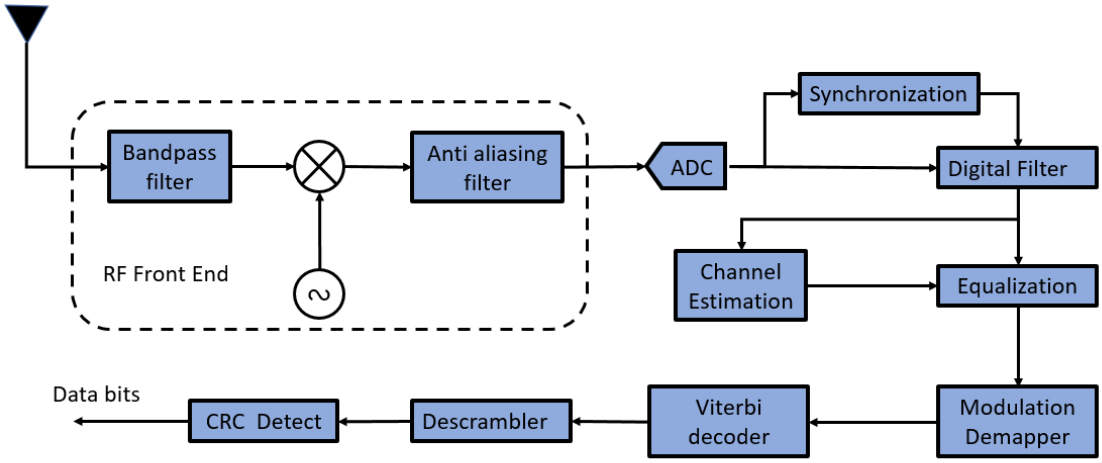

Figure 4.1: Basic receiver block diagram

4.1 RF Front End

The RF front end typically consists of all the signal processing blocks between the antenna and the digital baseband system. Since, the signal processing done in these blocks happen in the analog domain, RF front end is sometimes also referred

to as analog front end. Bandpass filter, low noise amplifier (LNA), mixer, baseband filters are some of the basic blocks in the RF front end. There are numerous receiver RF front end architectures such as: Super-Heterodyne receiver, Zero-IF (homodyne) receiver, Low-IF receiver, Band-pass sampling receiver etc [36]. Going into details of these architectures is beyond the scope of the thesis and we'll limit our discussion to the signal processing to be done by any of the chosen architecture.

An RF band-pass filter locks to a frequency band around the carrier frequency and captures the frequencies which lie inside the band while rejecting any signal outside the band. The captured signal is then down-converted from the carrier frequency to the baseband frequency with the help of a mixer. To prevent aliasing, a low pass analog filter further filters out the out-of-band energy from the signal before it is converted to digital samples by an ADC.

Since, the desired signal in the proposed system occupies a very narrow bandwidth of 15 kHz, it is desired to have a very narrow bandpass filter around the sub-carrier frequency. However, very narrow-band filters with sharp cutoff are highly complex and expensive, so we choose to allow some leakage from the adjacent sub-carriers. A mixer then down-converts the signal to baseband by mixing the filtered signal with the subcarrier frequency. The baseband signal thus obtained is then converted to digital samples by passing it through an ADC. The sampling rate of the ADC is kept a little higher (about eight times oversampled) to prevent aliasing because of the energy leakage from the adjacent subcarriers.

4.2 Synchronization

When a UE is powered on, the first task is to perform a cell search and detect a suitable cell to camp on and obtain the timing and frequency synchronization parameters, such as frame boundary, subframe boundary, carrier frequency etc. It also

needs to detect and correct frequency and timing offsets, if any, to prevent ISI and ICI which degrades the system performance.

Synchronization in LTE is carried out by making use of the synchronization signals - PSS and SSS which are known to the receiver. NB-IoT uses NPSS and NSSS sequences for synchronization. A number of methods have been proposed in the literature for a low cost implementation of the synchronization process for LTE [37–41] and NB-IoT [42–45].

The proposed VNB-IoT uses the same base sequence as in NB-IoT but with an extended code cover sequence. Since, the receiver has a very narrow bandwidth of 15kHz comprising of a single sub-carrier, only a single symbol from the base sequence, multiplied by the code cover sequence is received at the receiver. The constant-amplitude zero-autocorrelation (CAZAC) property of the code cover sequence allows to implement a matched filter based detector. Various optimizations can be done to reduce the complexity and power consumption of the synchronizer.

4.3 Channel Estimation and Equalization

Like LTE and NB-IoT, VNB-IoT also uses the CRS to estimate channel frequency response at given locations in each subframe. The estimation process is carried out as described in Section 2.5 using one of the standard zero forcing (ZF) or minimum mean-squared error (MMSE) based estimation techniques. However, there are numerous other methods of channel estimation researched in the past [46–48].

Interpolation techniques are then used to estimate the channel over rest of the symbols in the subframe . The channel response coefficients thus obtained are used to equalize the received symbols by employing a single tap frequency domain equalizer.

4.4 Demodulation and decoding

The equalized symbols are mapped to one of the constellation points, depending on the modulation scheme used. The output of the demodulator is then passed to a descrambler, which undoes the scrambling process performed at the transmitter. Demapping and descrambling can either be soft or hard. In hard decision demapping, the bits corresponding to the chosen constellation point are passed to the descrambler while in soft decision based demapping likelihood ratios are calculated. The scrambler's output is passed to a viterbi decoder which corrects the channel errors occurred during the transmission and extract the payload bits. Similar to demapper and descrambler, viterbi decoder can also be based on either hard or soft decisions.

Chapter 5

SIMULATIONS AND RESULTS

All the previous chapters described the problem statement, underlying principles, transmitter and receiver architecture of the proposed VNB-IoT system. This chapter presents a MATLAB® based, basic simulation model to analyze the performance of the proposed wireless system along with the simulation methods used and the results obtained during the study. We first discuss the filter selection process for both analog and digital filters for our simulations. Next, the bit-error-rate (BER) performance of our system under AWGN channel conditions is studied followed by an experimental analysis of interference noise power. Finally, we consider the system under a Rayleigh fading channel with equalization.

5.1 Filter Selection

Our system involves three main filters - an analog band pass filter and two digital downsampling filters. For the sake of convenience, we model the analog bandpass filter by using a digital low pass filter after down-converting the signal to baseband. All the filers chosen for our study are implemented as constrained equiripple finite impulse response (FIR) filters having a passband ripple of 0.01 and stopband rejection of 50 dB. We discuss below, the characteristics of all the three filters chosen for the study.

5.1.1 Analog Bandpass Filter

As discussed before, we design our bandpass filter around the sub-carrier of interest such that it allows a maximum of three subcarriers on either side to leak energy in

band, i.e. we want the fourth adjacent subcarrier to be completely rejected. This would enable the ADC to run at critical sampling rate of 90kHz, but in order to avoid a sharp digital filter, we shall use an ADC running at a sampling rate of 120 kHz.

For a subcarrier spacing of 15 kHz, in order to completely suppress the fourth adjacent subcarrier, the analog filter should have a stopband edge of 60kHz. Since, there are twelve subcarriers in a resource block of NB-IoT, with 6 subcarriers on positive and negative side each will give a maximum frequency of 90kHz. This means that a sampling rate of 240 kHz is good enough to make sure there is no aliasing.

A typical down-conversion process involves a bandpass filter followed by a mixer. But for simulation purpose, we shall use a mixer first, followed by an analog low pass filter. The mixer will be tuned to the frequency corresponding to the desired subcarrier, and hence brings the desired subcarrier to the DC. The analog bandpass filter is implemented as a digital low pass filter, after moving the desired subcarrier to DC. We believe that reversing the order of mixer and filter would not have any impact on the system performance in terms of BER.

Figure Figure 5.1 shows the magnitude response of the filter. The length 12 filter, having a stopband edge at 60 kHz, suppresses the 4th adjacent subcarrier on either side of the DC by about 50 dB. The filter output is downsampled by a factor of 2 so that the ADC operates at a sampling rate of 120 kHz.

5.1.2 Digital Lowpass Filters

Figure Figure 5.2 represents the magnitude responses of the two digital filters used for the simulation. The first filter has a stopband edge around 30 kHz and hence leaves only one adjacent subcarrier interfering with our subcarrier at DC. The samples are downsampled by a factor of 2 to obtain a sampling rate of 60kHz. The second digital filter suppresses the adjacent subcarrier at 15 kHz by around 40 dB. The filter output

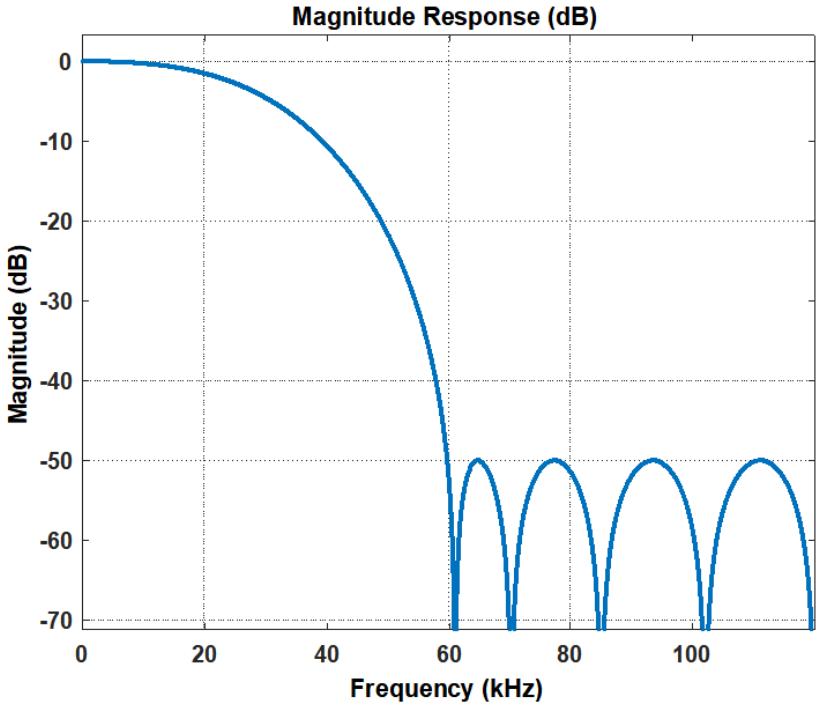

Figure 5.1: Magnitude response of the analog filter

is downsampled by 5 to obtain a single sample per symbol. Choosing the sample with an offset of 3 will ensure a significant reduction in ISI caused due to filter delay.

The filter designs discussed above may not be the best designs possible. These filters are selected just to study the performance of the system. Optimizations can be done in design and process to further reduce the complexity of the system.

5.2 Performance in AWGN

We begin with analyzing the BER performance of the system in an AWGN channel for two modulation schemes - BPSK and QPSK. To study the fundamental behavior of the system, we shall not use any coding or scrambling blocks. As a first experiment, we transmit data only on the desired subcarrier and send no information on rest of the subcarriers. This is similar to transmitting data over a single frequency.

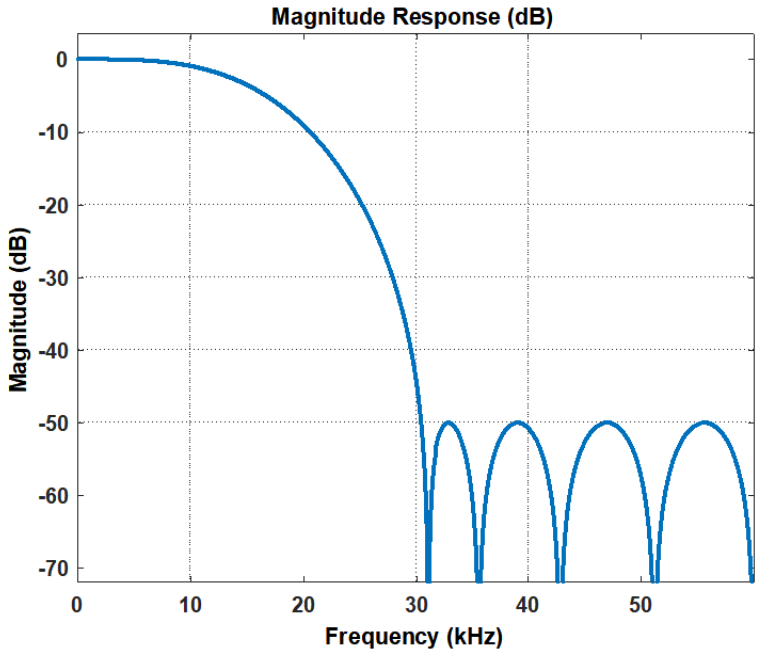

(a)

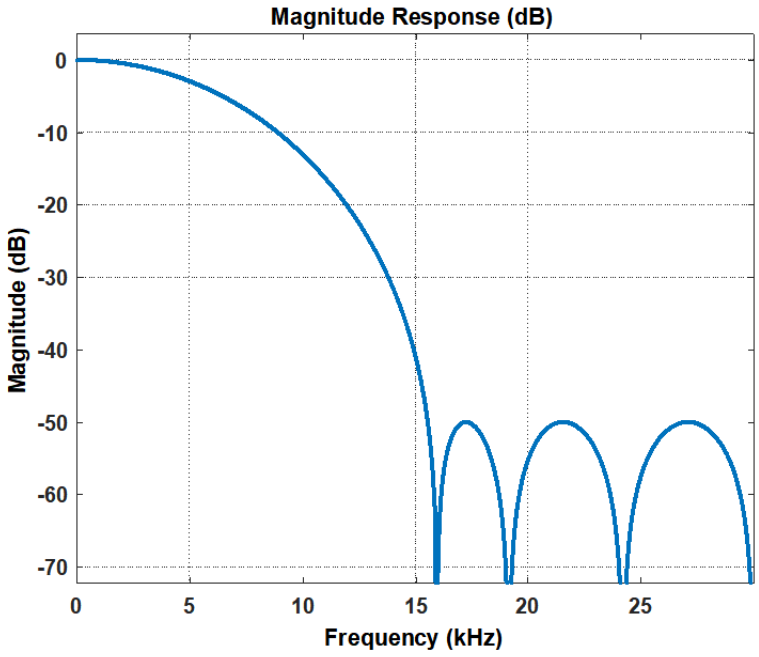

(b)

Figure 5.2: Magnitude response (a) Digital Filter 1 (b) Digital Filter 2

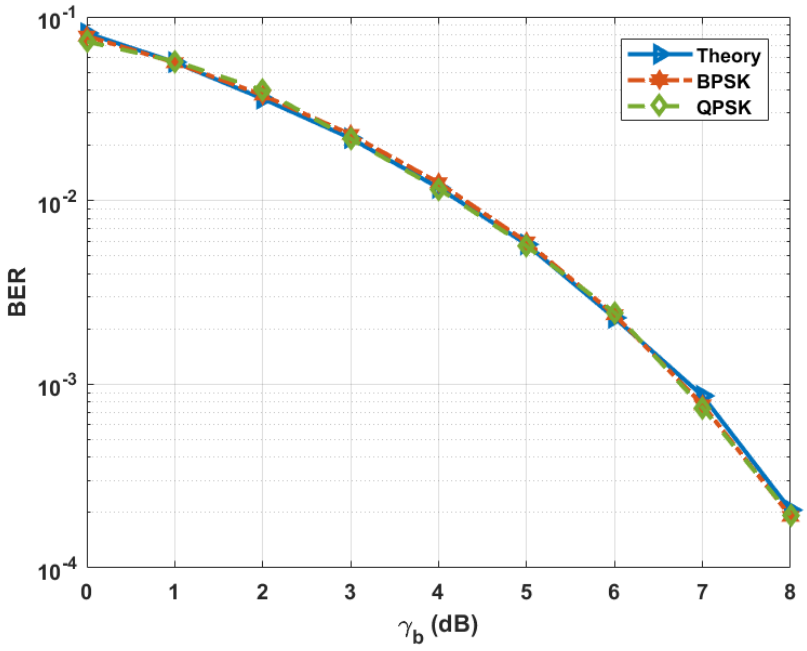

Figure 5.3: Probability of bit error,P_b vs E_b/N_0 for BPSK and QPSK modulation with adjacent subcarriers transmitted as nulls

As shown in Figure 5.3, the performance for both, BPSK and QPSK, match the theoretical performance for a conventional single carrier transmission given by [11]:

$$P_b = Q(\sqrt{2\gamma_b}) \tag{5.1}$$

where P_b is the probability of bit-error, SNR per bit, $\gamma_b = \frac{E_b}{N_0}$, E_b and N_0 being the energy per bit and noise power spectral density (PSD), and the Q-function is defined as

$$Q(x) = \frac{1}{\sqrt{2\pi}} \int_x^\infty e^{-\frac{x^2}{2}} dx \tag{5.2}$$

Next, we transmit the OFDM symbols with adjacent subcarriers loaded with data. Figure 5.4 shows degradation in the BER performance for both BPSK and QPSK as compared to the theoretical performance. This degradation can be attributed to the interference from the adjacent subcarriers, leaking because of the filter roll-off.

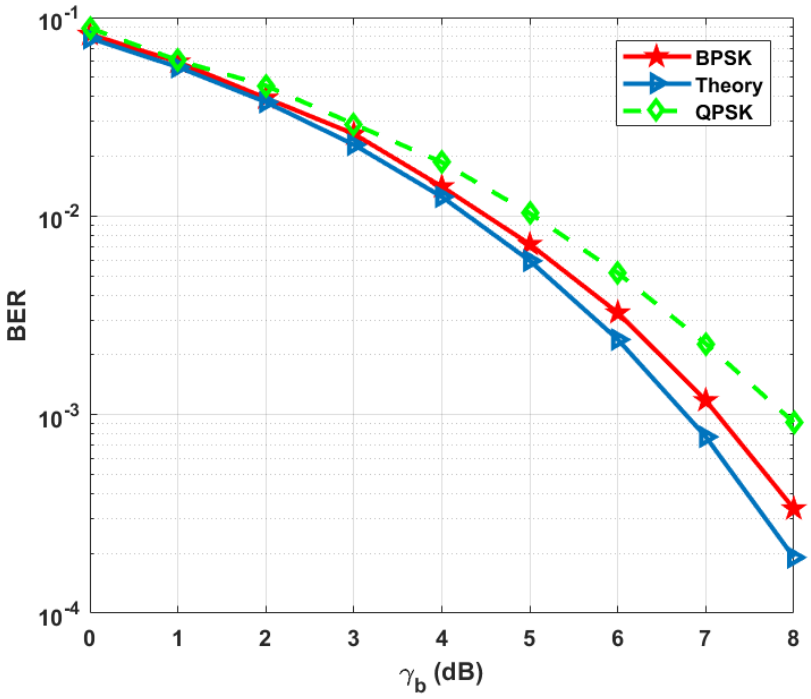

Figure 5.4: Probability of bit error,P_b vs E_b/N_0 for BPSK and QPSK modulation

To verify this fact, we analyze the constellation diagrams for both, BPSK (Figure 5.5) and QPSK (Figure 5.6) modulated symbols. We see that the received constellations are scattered even without adding any gaussian noise.

Further, we observe that the interference looks like a zero-mean Gaussian noise around the transmitted constellation. Next, we estimate the SNR obtained because of the interference noise for the given set of filters as, [49]

$$SNR = \frac{|R_{S\overline{Z}}|^2}{< |Z_n|^2 >< |S_n|^2 > -|R_{S\overline{Z}}|^2} \tag{5.3}$$

where S_n and Z_n are the transmitted and received modulation symbols, respectively, in the n^{th} OFDM symbol and $R_{S\overline{Z}}$ is the cross-correlation of S_n and Z_n, defined as

$$R_{S\overline{Z}} =< S_n Z_n^* > \tag{5.4}$$

where $< . >$ denotes the expectation operator and $(.)^*$ represents complex conjugate.

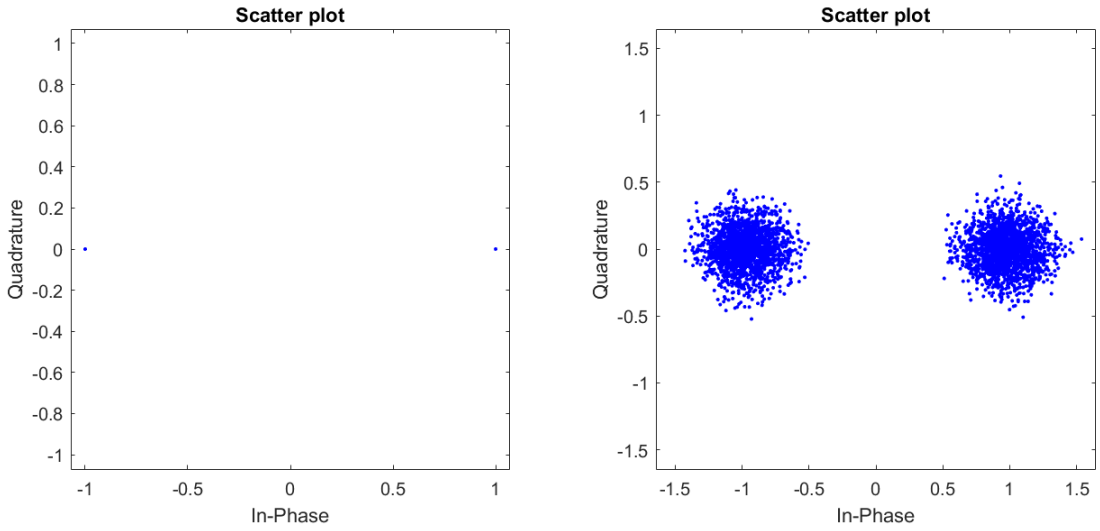

(a) (b)

Figure 5.5: Constellation of transmitted and received symbols for BPSK modulation

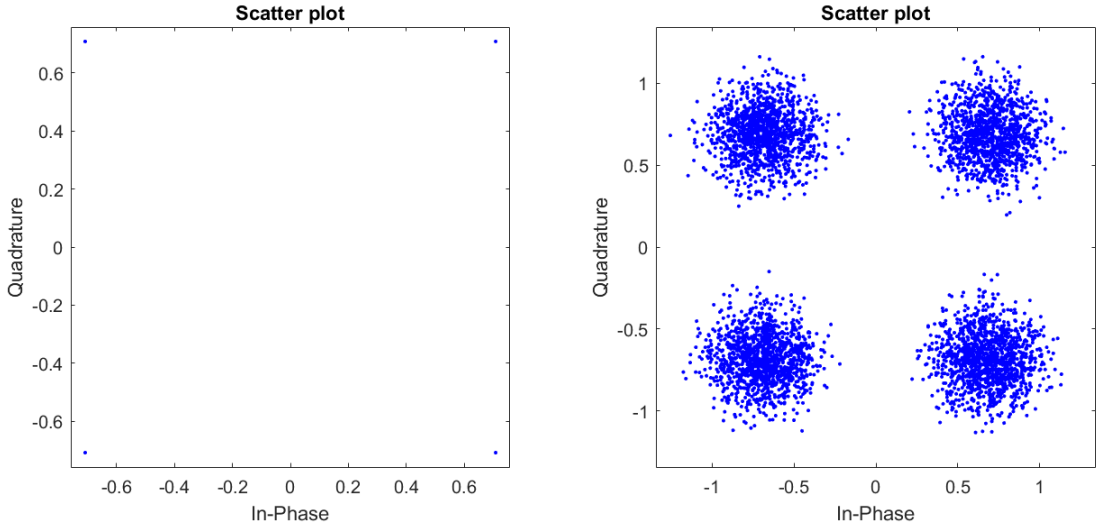

(a) (b)

Figure 5.6: Constellation of transmitted and received symbols for QPSK modulation

For transmitted symbol power, $< |S_n|^2 >= 1$, and with no AWGN noise added, interference noise variance can be calculated as, $N_I = \frac{1}{SNR}$. The effective SNR in an AWGN channel with interference, also known as SINR is then given by

$$SINR = \frac{E_b}{N_0 + N_I} \tag{5.5}$$

With the above relationship, we compare the BER performance with theoretical BER with the SNR being replaced by signal-to-interference-plus-noise ratio (SINR) (Figure 5.7). We observe that, the simulation performance curve is close to the theoretical curve justifying the fact that the degradation in performance is indeed because of the energy leaking from adjacent subcarriers and the interference can be assumed to be zero mean gaussian distributed. In the next section, we study how the interference changes with filter bandwidth.

5.3 Interference analysis

In the previous section, we found that energy from the adjacent subcarriers cause interference which has a zero-mean gaussian distribution and hence adds to the overall thermal noise floor. This interference depends on filter bandwidth as a wider filter will allow more interference from the adjacent subcarriers.

We define filter bandwidth as the range of frequencies over which the filter response lies within the 3dB range of its maximum value. The point on the frequency axis where the frequency response drops to half the maximum value is referred as the 3dB point. As the next experiment, we vary the filter bandwidth from 3 kHz to 13 kHz and then measure the SNR through simulations. In the absence of thermal noise, this SNR will be indicative of the interference noise added from the adjacent subcarriers.

As shown by the blue curve in Figure 5.8, we observe that the SNR increases as we reduce the filter bandwidth from 13 kHz, hits a maximum around 7.5 kHz, which

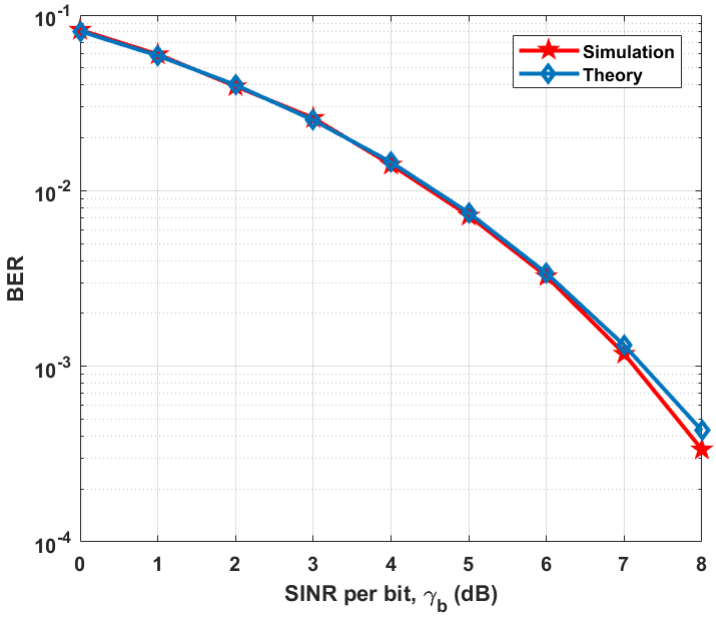

(a)

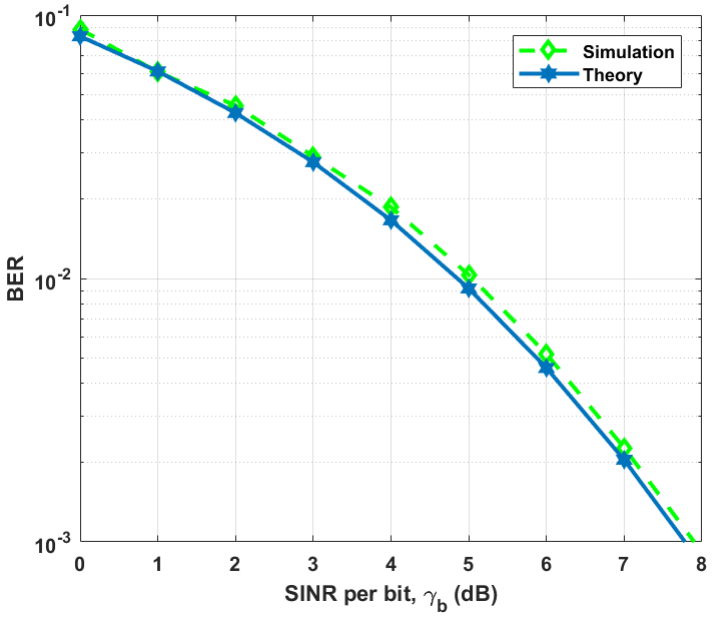

(b)

Figure 5.7: Probability of bit error,P_b vs SINR per bit, γ_b for (a) BPSK and (b) QPSK modulation

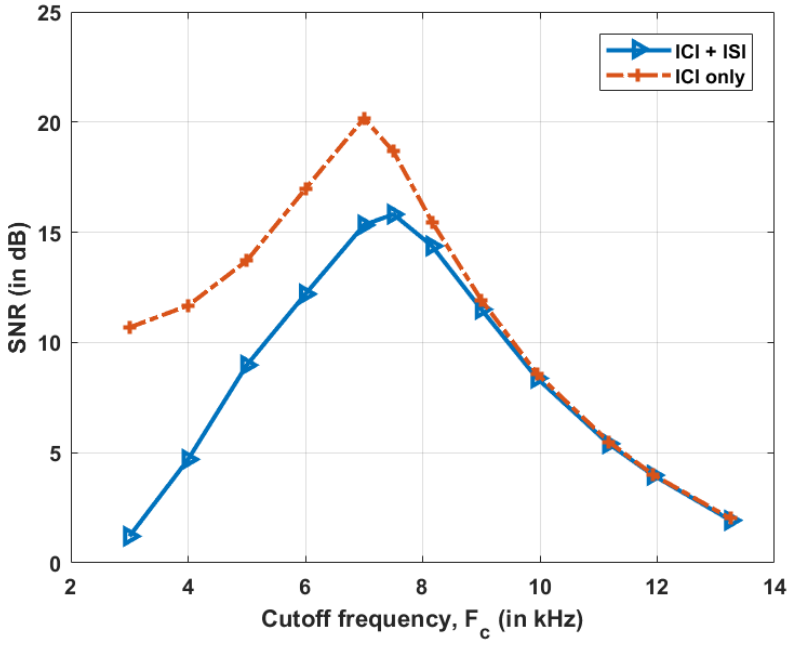

Figure 5.8: SNR vs overall filter cutoff frequency, F_c

is half the subcarrier spacing and then drops again as we further reduce the filter bandwidth. This drop in SNR for very narrowband filters is because of signal energy being filtered out by amount greater than noise. Thus, a filter with a bandwidth around 7.5kHz will be an optimum one to achieve the maximum SNR. The impulse response increase as the filter bandwidth decreases, resulting in a higher order filter. This leads to an increased smearing of the symbols in time domain leading to ISI. To see the effect of only ICI, we filter each symbol independently, so that there is no ISI. This would provide an estimate of the maximum SNR, that the system can achieve.

In Figure 5.8, the red curve shows how the SNR varies with filter bandwidth, when each symbol is filtered independently resulting in only ICI. A maximum SNR of about 20dB can be achieved by employing a filter with a bandwidth of half the sub-carrier spacing. This SNR cap is good for lower modulation schemes - BPSK and QPSK, as proposed in this thesis.

Chapter 6

CONCLUSION AND FUTURE WORK

In this work, we discussed the need to develop low cost wireless communication system for delay insensitive IoT applications demanding very low throughput. The wireless devices shall consume very less power and last for many years. We motivated the co-existence of such systems with the cellular network such as LTE. A single carrier based receiver architecture for downlink was developed by taking the resource allocation to one resource element per user and hence reaching the limit to multiple access. Performance of the proposed system was studied in AWGN and Rayleigh fading channel.

The work done in this thesis lays down the foundation in the development of wireless systems for IoT applications and can be further extended to develop a full-fledged communication system. Some of the future work that could be carried out as an extension to this thesis include:

- Extension of receiver design to process various data channels as mentioned in LTE.
- Development of better filters which consumes less power and allows less interference from the adjacent subcarriers
- Optimum synchronization signal design for robust initial acquisition and frequency and timing offset correction
- Reference signal design for channel estimation and tracking

REFERENCES

[1] Admin, "Introducing nb-iot technologies for cellular iot," *Digi,[Online]. Available: https://www.digi.com/blog/cellular/introducing-nb-iot-technologies-for-cellular-iot/.[Accessed 11 08 2017]*, 2017.

[2] J. Bradley, J. Barbier, and D. Handler, "Embracing the internet of everything to capture your share of $ 14.4 trillion," *White Paper, Cisco*, 2013.

[3] J. Morrish, E. Buckland, and M. Hatton, "Report-m2m global forecast and analysis 201122," *Annual Report, Machina Research*, 2013.

[4] R. Ratasuk, N. Mangalvedhe, and A. Ghosh, "Overview of lte enhancements for cellular iot," in *Personal, Indoor, and Mobile Radio Communications (PIMRC), 2015 IEEE 26th Annual International Symposium on*. IEEE, 2015, pp. 2293–2297.

[5] S. Sesia, M. Baker, and I. Toufik, *LTE-the UMTS long term evolution: from theory to practice*. John Wiley & Sons, 2011.

[6] E. Dahlman, S. Parkvall, J. Skold, and P. Beming, *3G evolution: HSPA and LTE for mobile broadband*. Academic press, 2010.

[7] Y.-P. E. Wang, X. Lin, A. Adhikary, A. Grövlen, Y. Sui, Y. Blankenship, J. Bergman, and H. S. Razaghi, "A primer on 3gpp narrowband internet of things (nb-iot)," *arXiv preprint arXiv:1606.04171*, 2016.

[8] R. Ratasuk, B. Vejlgaard, N. Mangalvedhe, and A. Ghosh, "Nb-iot system for m2m communication," in *Wireless Communications and Networking Conference (WCNC), 2016 IEEE*. IEEE, 2016, pp. 1–5.

[9] R. Ratasuk, N. Mangalvedhe, Y. Zhang, M. Robert, and J.-P. Koskinen, "Overview of narrowband iot in lte rel-13," in *Standards for Communications and Networking (CSCN), 2016 IEEE Conference on*. IEEE, 2016, pp. 1–7.

[10] D. R. J. Schlienz and D. Raddino, "Narrowband internet of things whitepaper," *Rode&Schwarz,[Online]. Available: https://cdn. rohde-schwarz. com/pws/dl_downloads/dl_application/application_notes/1ma266/1MA266_0e_NB_IoT. pdf.[Accessed 10 05 2017]*, 2016.

[11] A. Goldsmith, *Wireless communications*. Cambridge university press, 2005.

[12] T. S. Rappaport *et al.*, *Wireless communications: principles and practice*. prentice hall PTR New Jersey, 1996, vol. 2.

[13] D. Tse and P. Viswanath, *Fundamentals of wireless communication*. Cambridge university press, 2005.

[14] R. v. Nee and R. Prasad, *OFDM for wireless multimedia communications*. Artech House, Inc., 2000.

[15] X. Li and L. J. Cimini, "Effects of clipping and filtering on the performance of ofdm," in *Vehicular Technology Conference, 1997, IEEE 47th*, vol. 3. IEEE, 1997, pp. 1634–1638.

[16] S. H. Muller and J. B. Huber, "A comparison of peak power reduction schemes for ofdm," in *Global Telecommunications Conference, 1997. GLOBECOM'97., IEEE*, vol. 1. IEEE, 1997, pp. 1–5.

[17] L. J. Cimini and N. R. Sollenberger, "Peak-to-average power ratio reduction of an ofdm signal using partial transmit sequences," *IEEE Communications letters*, vol. 4, no. 3, pp. 86–88, 2000.

[18] R. W. Bauml, R. F. Fischer, and J. B. Huber, "Reducing the peak-to-average power ratio of multicarrier modulation by selected mapping," *Electronics letters*, vol. 32, no. 22, pp. 2056–2057, 1996.

[19] J. Tellado, *Multicarrier modulation with low PAR: applications to DSL and wireless*. Springer Science & Business Media, 2006, vol. 587.

[20] T. M. Schmidl and D. C. Cox, "Robust frequency and timing synchronization for ofdm," *IEEE transactions on communications*, vol. 45, no. 12, pp. 1613–1621, 1997.

[21] J.-J. Van de Beek, M. Sandell, and P. O. Borjesson, "Ml estimation of time and frequency offset in ofdm systems," *IEEE transactions on signal processing*, vol. 45, no. 7, pp. 1800–1805, 1997.

[22] H. Bolcskei, "Blind estimation of symbol timing and carrier frequency offset in wireless ofdm systems," *IEEE Transactions on Communications*, vol. 49, no. 6, pp. 988–999, 2001.

[23] H. Minn, M. Zeng, and V. K. Bhargava, "On timing offset estimation for ofdm systems," *IEEE Communications letters*, vol. 4, no. 7, pp. 242–244, 2000.

[24] J.-J. Van de Beek, P. O. Borjesson, M.-L. Boucheret, D. Landstrom, J. M. Arenas, P. Odling, C. Ostberg, M. Wahlqvist, and S. K. Wilson, "A time and frequency synchronization scheme for multiuser ofdm," *IEEE Journal on selected areas in communications*, vol. 17, no. 11, pp. 1900–1914, 1999.

[25] B. Furht and S. A. Ahson, *Long Term Evolution: 3GPP LTE radio and cellular technology*. Crc Press, 2016.

[26] C. Cox, *An introduction to LTE: LTE, LTE-advanced, SAE and 4G mobile communications*. John Wiley & Sons, 2012.

[27] E. Dahlman, S. Parkvall, and J. Skold, *4G: LTE/LTE-advanced for mobile broadband*. Academic press, 2013.

[28] D. Flore, "3gpp standards for the internet-of-things," *Recuperado el*, vol. 25, 2016.

[29] Y.-H. Nam, Y. Akimoto, Y. Kim, M.-i. Lee, K. Bhattad, and A. Ekpenyong, "Evolution of reference signals for lte-advanced systems," *IEEE Communications Magazine*, vol. 50, no. 2, 2012.

[30] A. Ghosh, R. Ratasuk, B. Mondal, N. Mangalvedhe, and T. Thomas, "Lte-advanced: next-generation wireless broadband technology," *IEEE wireless communications*, vol. 17, no. 3, 2010.

[31] S. Parkvall, E. Dahlman, A. Furuskar, Y. Jading, M. Olsson, S. Wanstedt, and K. Zangi, "Lte-advanced-evolving lte towards imt-advanced," in *Vehicular Technology Conference, 2008. VTC 2008-Fall. IEEE 68th.* IEEE, 2008, pp. 1–5.

[32] D. Astély, E. Dahlman, A. Furuskär, Y. Jading, M. Lindström, and S. Parkvall, "Lte : The evolution of mobile broadband," *IEEE Communications magazine*, vol. 47, no. 4, 2009.

[33] R1-161981, "Nb-pss and nb-sss design (revised)," *Qualcomm, 3GPP RAN WG1 NB-IoT Ad-Hoc Meeting, Mar. 22-24*, 2016.

[34] R1-157068, "Design principles of nb-iot sync channel," *Qualcomm, 3GPP RAN1 Meeting 83, Nov. 15-22*, 2015.

[35] R1-157069, "Sequence design for nb-iot sync channel," *Qualcomm, 3GPP RAN1 Meeting 83, Nov. 15-22*, 2015.

[36] P. Cruz, H. Gomes, and N. Carvalho, "Receiver front-end architectures–analysis and evaluation," in *Advanced Microwave and Millimeter Wave Technologies Semiconductor Devices Circuits and Systems.* InTech, 2010.

[37] W. Xu and K. Manolakis, "Robust synchronization for 3gpp lte system," in *Global Telecommunications Conference (GLOBECOM 2010), 2010 IEEE.* IEEE, 2010, pp. 1–5.

[38] L.-C. Wung, Y.-C. Lin, Y.-J. Fan, and S.-L. Su, "A robust scheme in downlink synchronization and initial cell search for 3gpp lte system," in *Wireless and Pervasive Computing (ISWPC), 2011 6th International Symposium on.* IEEE, 2011, pp. 1–6.

[39] K. Manolakis, D. M. G. Estévez, V. Jungnickel, W. Xu, and C. Drewes, "A closed concept for synchronization and cell search in 3gpp lte systems," in *Wireless Communications and Networking Conference, 2009. WCNC 2009. IEEE.* IEEE, 2009, pp. 1–6.

[40] X. Yang, Y. Xiong, G. Jia, W. Fang, and X. Zheng, "Pss based time synchronization for 3gpp lte downlink receivers," in *Communication Technology (ICCT), 2011 IEEE 13th International Conference on.* IEEE, 2011, pp. 930–933.

[41] Y. Gao, G. Zhu, X. Chen, D. Wu, and B. Ban, "A modified algorithm of synchronization signal detection for lte initial cell search," in *Communications and Networking in China (CHINACOM), 2011 6th International ICST Conference on.* IEEE, 2011, pp. 1211–1215.

[42] A. Ali and W. Hamouda, "On the cell search and initial synchronization for nb-iot lte systems," *IEEE Communications Letters*, 2017.

[43] H. Kroll, M. Korb, B. Weber, S. Willi, and Q. Huang, "Maximum-likelihood detection for energy-efficient timing acquisition in nb-iot," in *Wireless Communications and Networking Conference Workshops (WCNCW), 2017 IEEE*. IEEE, 2017, pp. 1–5.

[44] W. Yang, M. Hua, J. Zhang, T. Xia, J. Zou, C. Jiang, and M. Wang, "Enhanced system acquisition for nb-iot," *IEEE Access*, vol. 5, pp. 13 179–13 191, 2017.

[45] E. Jörgensen, "Cell acquisition and synchronization for unlicensed nb-iot," 2017.

[46] A. Ancora, C. Bona, and D. T. Slock, "Down-sampled impulse response least-squares channel estimation for lte ofdma," in *Acoustics, Speech and Signal Processing, 2007. ICASSP 2007. IEEE International Conference on*, vol. 3. IEEE, 2007, pp. III–293.

[47] X. Dai, W. Zhang, J. Xu, J. E. Mitchell, and Y. Yang, "Kalman interpolation filter for channel estimation of lte downlink in high-mobility environments," *EURASIP Journal on Wireless Communications and Networking*, vol. 2012, no. 1, p. 232, 2012.

[48] L. A. M. R. de Temino, C. N. i Manchon, C. Rom, T. B. Sorensen, and P. Mogensen, "Iterative channel estimation with robust wiener filtering in lte downlink," in *Vehicular Technology Conference, 2008. VTC 2008-Fall. IEEE 68th.* IEEE, 2008, pp. 1–5.

[49] S. He and M. Torkelson, "Effective snr estimation in ofdm system simulation," in *Global Telecommunications Conference, 1998. GLOBECOM 1998. The Bridge to Global Integration. IEEE*, vol. 2. IEEE, 1998, pp. 945–950.

APPENDIX A

LIST OF ACRONYMS

ACI adjacent channel interference

ADC analog-to-digital converter

AWGN additive white Gaussian noise

BPSK binary phase-shift keying

BER bit-error-rate

CAZAC constant-amplitude zero-autocorrelation

CDMA Code division multiple access

CRC cyclic-redundancy-check

CRS cell-specific reference signal

CSMA Carrier sense multiple access

DAC digital-to-analog converter

FDM frequency division multiplexing

FDMA Frequency division multiple access

GSM Global System for Mobile Communications

IFFT inverse fast-fourier-transform

ISI inter symbol interference

LTE Long-Term Evolution

MAC multiple access channel

MMSE minimum mean-squared error

OFDM orthogonal frequency division multiplexing

OFDMA Orthogonal frequency division multiple access

PAPR peak-to-average power ratio

PBCH Physical Broadcast Channel

PDCCH Physical Downlink Control Channel

PDSCH Physical Downlink Shared Channel

PSK phase-shift-keying

QPSK quadrature phase-shift keying

SDMA Space division multiple access

SINR signal-to-interference-plus-noise ratio

SNR signal-to-noise ratio

TDMA Time division multiple access

UE user equipment

ZF zero forcing

IoT Internet of Things

M2M machine to machine

MTC machine type communication

LTE Long Term Evolution

3GPP 3rd generation partnership project

NB-IoT narrowband Internet of Things (IoT)

VNB-IoT very narrowband IoT

GSM global gystem for mobile communication

RB resource block

FFT Fast Fourier Transform

PSS primary synchronization sequence

NPSS narrowband primary synchronization sequence (PSS)

SSS secondary synchronization sequence

NSSS narrowband secondary synchronization sequence (SSS)

ICI inter-(sub)carrier-interference

LAN local area network

WAN wide area network